JOURNAL OF AIRCRAFT
Vol. 41, No. 5, September–October 2004

Numerical Study of Blowing and Suction Control Mechanism on NACA0012 Airfoil

L. Huang,* P. G. Huang,† and R. P. LeBeau‡
University of Kentucky, Lexington, Kentucky 40506-0108
and
T. Hauser§
Utah State University, Logan, Utah 84322-4130

A jet with a width of 2.5% the chord length is placed on a NACA0012 airfoil's upper surface simulating the blowing and suction control under $Re = 5 \times 10^5$ and angle-of-attack 18-deg conditions. Nearly 300 numerical simulations are conducted over a range of parameters (jet location, amplitude, and angle). The physical mechanisms that govern suction and blowing flow control are determined and analyzed, and the critical values of suction and blowing locations, amplitudes, and angles are discussed. The current successful large-scale numerical studies create a useful knowledge base for further exploration of multijet control system.

Nomenclature

A	=	suction or blowing amplitude, $\lvert V_j \rvert / u_\infty$
A_H	=	height of computation area
A_W	=	width of computation area
C_d	=	drag coefficient, $D/q_0 c$
C_{dB}	=	drag coefficient of baseline case(without suction/blowing)
C_l	=	lift coefficient, $L/q_0 c$
C_{lB}	=	lift coefficient of baseline case (without suction/blowing)
C_p	=	pressure coefficient, $(P - P_0)/q_0$
c	=	airfoil chord length
h	=	suction/blowing jet width, defined as 2.5% chord length
L_j	=	jet position on the airfoil's surface, streamline distance start from leading edge
q_0	=	freestream dynamic pressure, $\frac{1}{2}\rho u_\infty^2$
Re	=	Reynolds number
s	=	streamline axis along airfoil surface, start at leading edge
u_∞	=	freestream velocity
V_j	=	velocity at suction or blowing jet entrance
x	=	x axis
x'	=	axis parallel to chord line
y	=	y axis
y'	=	distance normal to x' axis
α	=	angle of attack
β	=	angle between freestream velocity direction and local jet surface
Γ	=	circulation
θ	=	suction or blowing angle, −90 deg as perpendicular suction, 90 deg as perpendicular blowing, measure from the local jet surface
ν	=	dynamic viscosity
ρ	=	air density

Received 6 May 2003; revision received 13 October 2003; accepted for publication 15 October 2003. Copyright © 2003 by the American Institute of Aeronautics and Astronautics, Inc. All rights reserved. Copies of this paper may be made for personal or internal use, on condition that the copier pay the $10.00 per-copy fee to the Copyright Clearance Center, Inc., 222 Rosewood Drive, Danvers, MA 01923; include the code 0021-8669/04 $10.00 in correspondence with the CCC.

*Graduate Research Assistant, Mechanical Engineering. Student Member AIAA.
†Professor, Mechanical Engineering. Senior Member AIAA.
‡Assistant Professor, Mechanical Engineering. Member AIAA.
§Assistant Professor, Mechanical and Aerospace Engineering. Member AIAA.

Introduction

EARLY works[1–3] in the airfoil control area primarily emphasized passive methods such as modifying the geometric shapes to maneuver the pressure gradient, thereby delaying turbulence and preventing separation over the airfoil's upper (low-pressure) surface. Although a sound idea, the end results are not always adequate, in as much as they are limited by the playground of the airfoil geometry. An alternative approach was active flow control, which significantly changed the lift by injecting a small amount of energy into the system to control the development of the boundary layer. Suction and blowing techniques emerged and have been studied in a variety of experiments.[4,5] These experiments demonstrated that suction and blowing can actively modify the pressure distribution over an airfoil surface and lead to a dynamic virtual shaping.

In previous decades, numerous experiments were performed on the most common NACA airfoils, measuring lift and drag coefficients under different flow conditions. However, under some conditions even this type of simple measurement can yield wind-tunnel data with a wide range of scatter. In these cases, the addition of suction and blowing controls to these systems will paradoxically require finer measurements of sensitive, smaller scale flows while increasing the complexity of the overall flow and further increasing the likelihood of experimental error. Trying to repeat these experiments over a wide range of potential parameters necessary to determine the optimal performance conditions for an active flow control design would necessarily be expensive; systematically isolating the multiple factors and fine-flow structures that potentially govern the behavior of the active flow systems through experiments is nearly impossible.

The alternative approach is numerical simulation, which, in the proper context, is more affordable, practical, systematic, and reliable. Numerical simulation can provide a deeper understanding inside the control mechanisms and can lead to the discovery of critical fluid phenomena and pattern changes. Understanding these suction[6] and blowing flow control mechanisms will yield a more meaningful understanding of novel active flow control applications[7] and their numerical simulations[8–10]. Whereas there is a body of previous research targeting the ability of computational fluid dynamics (CFD) to simulate qualitatively active flow control systems, these results are limited to a small interest area and parameter scope, in which control properties had been studied only on the leading edge. The control effects in other locations and of other parameters (amplitude, angle) are less discussed and studied, but this missing information is also important to understand control mechanisms. The situation is partially due to the computational cost of simulating many cases. However, the growth of commodity computer clusters and techniques for distributed CFD have allowed us to transfer much of the

work from traditional supercomputer mainframes to relatively inexpensive groups of personal computers linked by a dedicated network. Series of numerical prototype test computations for a novel design concept can now be conducted on such a cluster, making large-scale and extensive numerical studies of active flow control prototypes increasingly practical.[11] In the current paper, we performed nearly 300 numerical simulations to discover the mechanisms underlying the suction and blowing control effects on a NACA0012 airfoil. Different driving factors are classified, and their contributions are measured and analyzed. With further qualitatively testing of computation results by experiments, this approach could form a useful information base for future multijet control system design.

Case Setup

Numerical Scheme

All present computations were performed with the CFD code GHOST. GHOST is an in-house CFD code developed at University of Kentucky by Huang. The code is based on a finite volume structured formulation with chimera overset grids. The QUICK and total variation diminishing schemes are applied to discretize the convective terms in the momentum and turbulence equations, respectively; the central difference scheme is used for the diffusive terms and the second-order upwind time discretization is employed for the temporal terms. This code has been tested extensively and is routinely used for turbulence model validation.[12–14] The turbulence model used in the present computation is Menter's shear stress transport two-equation model,[15] which provides excellent predictive capability for flows with separation.[16] The multiblock and chimera features of the code allow the use of fine-gird patches near the jet entrance and in regions of highly active flow. The code also employs message passing interface parallelization to allow different computational zones to be solved on different processors. Current computations are performed on the personal computer cluster KFC2 (48 Athlon 2000+ XP CPU), constructed by the CFD group at the University of Kentucky.

The Reynolds number being investigated in present computations is 5×10^5; therefore, a fully turbulent flow is reasonably assumed and no transition is involved in the computation. Because the focus of the current investigation is the control of the flow separation through blowing and suction jets, an incompressible Navier–Stokes solver is used to eliminate additional uncertainties caused by compressibility effects.

Grid Setup

The basic grid studies without jets implemented on the airfoil are setup as 15, two-dimensional multizonal blocks (Fig. 1). The grid of the NACA0012 airfoil is decomposed into four blocks (blocks 6–9), overlapping on three background blocks; another eight peripheral blocks surround the three background blocks. The dimensionless outer boundary of the computational area is choosen as $A_H \times A_W = 12c \times 12c = 12.0 \times 12.0$, large enough to prevent the outer boundary from affecting the near flowfield around the airfoil.

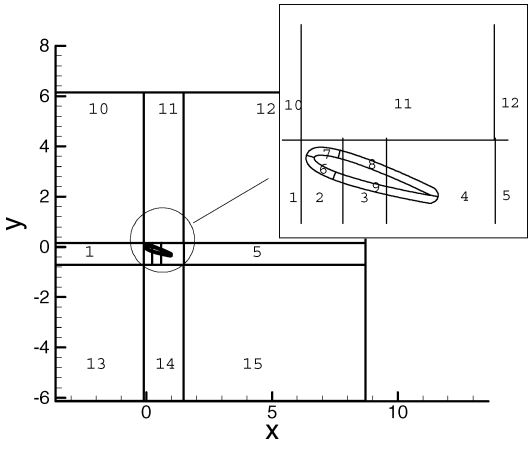

Fig. 1 Multizonal (blocks) grid, total of 15 blocks.

Table 1 Coarse grid and dense grid comparison

Block number	$1(i \times j)$	$2(i \times j)$	$3(i \times j)$
1	55×70	110×140	110×200
2 (background)	70×70	140×140	200×200
3 (background)	55×70	110×140	150×200
4 (background)	70×70	140×140	200×200
5	55×70	110×140	110×200
6 (airfoil)	54×25	107×50	148×75
7 (airfoil)	54×25	107×50	148×75
8 (airfoil)	70×25	120×50	220×75
9 (airfoil)	70×25	120×50	220×75
10	55×70	110×140	110×140
11	70×70	140×140	140×140
12	55×70	110×140	110×140
13	70×70	110×140	110×140
14	70×70	140×140	140×140
15	55×70	110×140	110×140

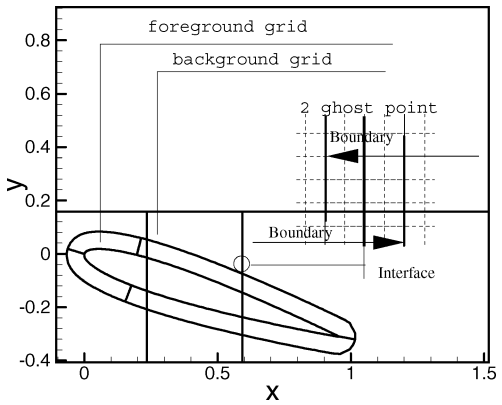

Fig. 2 Layout of foreground grid and background grid, where four foreground airfoil blocks overlap on three background blocks; information in the covered area of the background blocks interpolated from the foreground blocks, adjacent block information exchanged by two ghost points.

On the outer boundary, the left (inlet) boundary is fixed with a uniform dimensionless inlet velocity $u_\infty = 1.0$, the upper and lower boundary condition are freestream boundaries that satisfy the Neumann condition, and the right (outflow) boundary condition is set to a zero velocity gradient condition. For the airfoil blocks, the inner boundary condition is a no-slip wall boundary condition, and the outside boundary is set to overlap, which allows the background grid points being overlapped by the airfoil block grid points to interpolate values from the foreground airfoil grid points. Computation information between adjacent blocks is exchanged by two ghost points (Fig. 2). All of the parameters chosen in the computation are dimensionless. A special attempt was made to ensure that the near-wall $y+$ values of the airfoil blocks were kept within 0.5.

Airfoil blocks and their background blocks are the most sensitive computation areas; hence, the number of grid points in these blocks is most critical. To test for grid independence, three sets of grids, with increasing grid density (labeled 1, 2, and 3), are studied, and their results are listed in Table 1. These grids are studied under a Reynolds number of 5×10^5, and computational results for different angles of attack are compared in Table 2 and Fig. 3. The differences in the computational results between set 1 and set 2, and between set 2 and set 3, are less than 2%. To maintain grid-resolution consistency at different jet locations and relatively high grid resolution at the jet (dimensionless jet width of 0.025, grid resolution of 0.001), the relatively dense grid of set 2 is adopted in the current computation.

Present overset, multiblock grids give us the freedom to zoom into the flowfield around the suction and blowing location to investigate the flow patterns and corresponding properties and to reserve the ability for future multijet interaction studies. The number of grid

Table 2 Coarse and dense grid C_l and C_d comparison

α	$1C_l$	$2C_l$	$3C_l$	$1C_d$	$2C_d$	$3C_d$
0	0.001041	0.001325	0.001044	0.015655	0.015959	0.015820
2	0.189010	0.189645	0.189743	0.017108	0.017373	0.017036
5	0.463010	0.462302	0.462325	0.024201	0.024530	0.024260
10	0.853619	0.855687	0.857277	0.052585	0.052528	0.052540
12	0.958216	0.969597	0.963591	0.071107	0.071038	0.068659
14	1.016713	1.022523	1.015824	0.095095	0.093348	0.089901
16	0.974193	0.996049	0.977925	0.124510	0.122691	0.118370
18	0.856149	0.875904	0.897605	0.168011	0.166208	0.169420

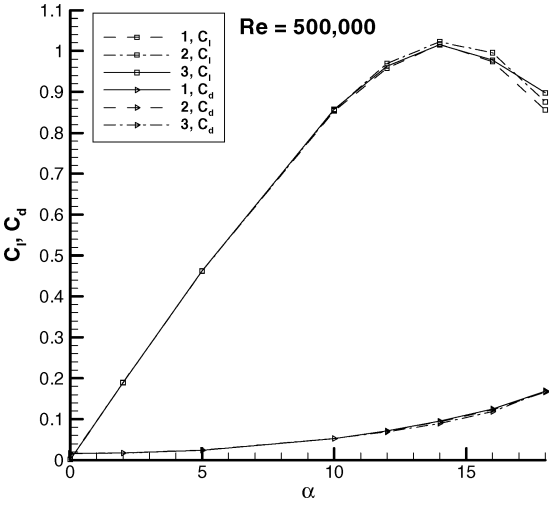

Fig. 3 Grid independence study of the grids in Table 1, $Re = 5 \times 10^5$.

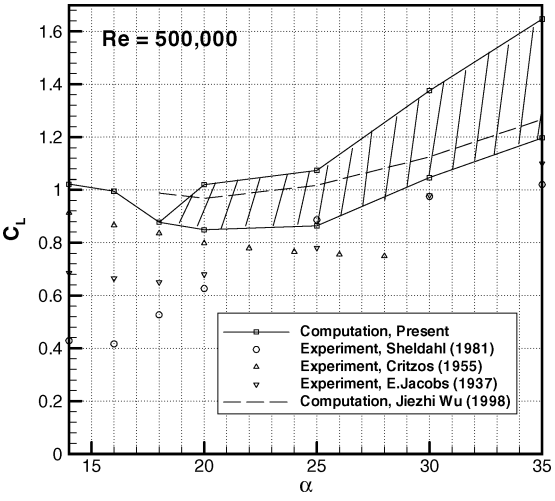

Fig. 4 Comparison between computation data and experiment data at $Re = 5 \times 10^5$.

points in set 2 is about 210,000 and the computation time is around 2 h on 15 processors for each case.

Even though the current paper mainly focuses on suction and blowing under an angle of attack of 18 deg, we do further computation beyond 18 deg to confirm the quality of our model. When started at an angle of attack of 20 deg, the lift and drag coefficient do not converge to a stable value; hence, a time-dependent version of GHOST is applied. The results vary periodically, which is similar to the result of Wu et al.[9] for large angle of attack. Therefore, in Fig. 4, computational results above 18 deg are plotted with an upper and lower value boundary; they are also compared to computational results of Wu et al. and three sets of experimental data,[17–19] all at $Re = 5 \times 10^5$.

It can be seen from Fig. 4 that the experimental data from sources 1, 2, and 3 vary widely, which implies a large amount of experimental uncertainty. This uncertainty is attributable to several factors. As suggested by numerous researchers, different flow regimes can occur depending on Reynolds number, angle of attack α, and airfoil geometry. Based on our literature survey of previous research, for the given NACA0012 airfoil at an angle of attack around 14 deg (a starting stall angle) and Reynolds number 5×10^5, the flow may fall into the low-frequency regime as proposed by Zaman et al.[20] where effects of both angle of attack and Reynolds number are strong. First, in the vicinity of an angle of attack at 14 deg (angles before the deep stall angle 18 deg), the flow can naturally switch between stall and nonstall and between steady attached and steady separated flow. Second, at $Re = 5 \times 10^5$ the flow regime is one where laminar separation is still possible. Therefore, this flow regime and its vicinity remain a challenge for both experimental measurement and computation prediction.

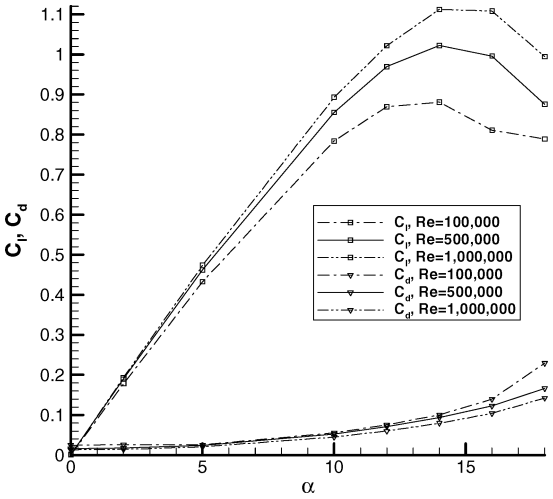

Fig. 5 Computation results at $Re = 1 \times 10^5$, 5×10^5, and 1×10^6.

Given these Reynolds number concerns and assuming no transition, computations have also been performed on both a lower and higher number than 5×10^5. Results at different Reynolds number in Fig. 5 demonstrate that the stall starts consistently around 14 deg. The maximum C_l of $Re = 5 \times 10^5$ and 1×10^6 are consistent with the maximum C_l of NACA TN-1945 cited by Wu et al.[9]; the C_l of $Re = 1 \times 10^5$ case is different from the proposed correlation value partly because no transition is assumed in present computation and partly because of the natural complexities of this regime.

In addition to the natural complexities and difficulties of this regime, the differences between the experiment and numerical simulation results over the NACA airfoil can also be attributed to other factors and errors that exist both on the experimental side and the numerical simulation side. On the experimental side, installation error in airfoil model, disturbance of measurement device, interference between wind-tunnel wall and airfoil body, freestream turbulence, and boundary-layer trips effects can create the errors of the measurement. On the numerical simulation side, turbulence models, artificial viscosity, grid density, and the limitations of two-dimensional simulation can produce computational inaccuracies. Also, different turbulence models, as well as their different combinations with various numerical schemes, could lead to qualitatively different predictions for separated flows. A detailed explanation of potential experimental errors may be found in the discussion of Jacobs and Sherman[19] and McCroskey,[21] and a heuristic discussion of numerical simulation limitations may be found by Wu et al.[9] Despite the challenges, the present computation results fall within the range of data used in previous published studies; therefore, we argue that these results can at least be used for qualitative understanding of the underlying flow physics and control mechanism.

Parameters Selection

Whereas most of the previous research has focused on suction or oscillatory blowing on the leading edge, studies about blowing and suction control separately in a wider scope are less frequent.

Table 3 Parameters of the four series of numerical simulations

Run	Jet location L_j	Amplitude A	Angle θ
First (64)	0.1, 0.333, 0.567, 0.8	0.01, 0.173, 0.337, 0.5	−90, −30, 30, 90
Second (32)	0.05, 0.075, 0.1, 0.125	0.01, 0.073, 0.137, 0.2	−90, −30
Third (64)	0.03, 0.04, 0.05, 0.06	0.01, 0.073, 0.137, 0.2	0_+, 30, 60, 90
Fourth (128)	0.2, 0.286, 0.371, 0.457, 0.543, 0.629, 0.714, 0.8	0.01, 0.073, 0.137, 0.2	0_+, 30, 60, 90

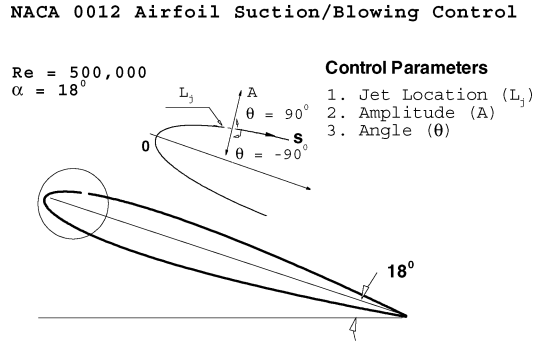

Fig. 6 Three control parameters: jet location L_j, amplitude A, and angle θ.

This information is important for understanding the basic control effects. Therefore, a sensitivity study of suction and blowing on the control of a NACA0012 airfoil is performed. Three parameters (Fig. 6) are selected in the current investigation, namely, jet location L_j, suction/blowing amplitude A, and suction/blowing angle θ. The jet width for both suction and blowing is fixed at 2.5% chord length based on a study[4] by Dannenberg and Weiberg, who showed that an increase of suction area beyond 2.5% chord length will not increase lift significantly.

In our numerical investigation, the jet entrance velocity is set as

$$u = A \cdot \cos(\theta + \beta), \qquad v = A \cdot \sin(\theta + \beta)$$

where β is the angle between the freestream velocity direction and the local jet surface, and θ is the angle between the local jet surface and jet entrance velocity direction. Note that negative θ represents suction condition and positive θ indicates blowing condition. For perpendicular suction, θ is −90 deg, and for a perpendicular blowing, θ is 90 deg. The range of jet entrance velocity amplitude is selected to be from 0.01 to 0.5 of freestream velocity. This range corresponds to a jet momentum coefficient C_μ,

$$C_\mu = \frac{\rho \cdot h \cdot v_j^2}{\rho \cdot c \cdot u_\infty^2} = \frac{h}{c} \cdot A^2$$

of 2.5×10^{-6} to 0.00625. It has been proposed[22] that a jet momentum coefficient C_μ around 0.002 is necessary to have some impact on the flow pattern. The jet location L_j is varied from 3 to 80% of the NACA0012 airfoil's upper surface. This range covers more of the airfoil length than those used in previous experimental and numerical studies. All cases are under Reynolds number 5×10^5 and angle-of-attack 18-deg conditions.

Results and Analysis

There are four rounds of numerical simulations performed in current study, and the computations are carried forward according to our target area of interest. The values chosen for each round are given in Table 3. To address the different mechanisms that govern suction and blowing, computation results for these two alternatives are presented and discussed separately.

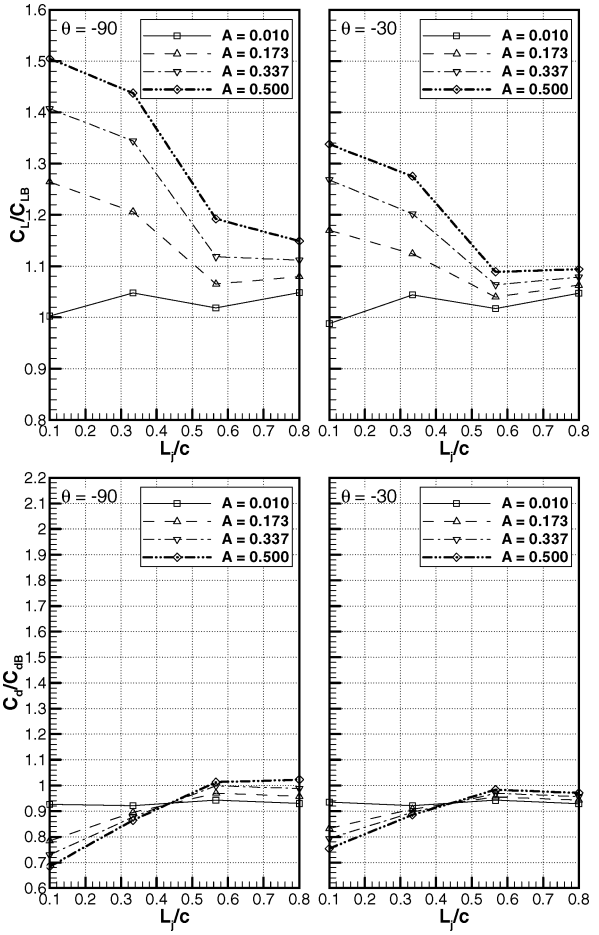

Fig. 7 Suction computation results of initial study, $0.1 \le L_j \le 0.8$, $0.01 \le A \le 0.5$, and $\theta = -90$ and -30 deg.

Suction Control

In Fig. 7, predicted lift and drag coefficients are compared for $0.01 < A < 0.5$, $0.1 < L_j < 0.8$, and $\theta = -90$ and -30 deg. The lift and drag coefficients are normalized by their corresponding values in the baseline case (no suction or blowing, $C_l = 0.875904$ and $C_d = 0.166208$ at $Re = 5 \times 10^5$ and $\alpha = 18$ deg). It can be concluded from these computation results that 1) perpendicular suction (−90 deg) has the largest impact on the increase of lift coefficient, 2) suction at location 0.1 is better than farther downstream, and 3) lift increases as suction amplitude increases above an amplitude of 0.01. Below 0.01, the flow does not appear to be significantly affected by the suction.

To further explore the flow control patterns of different locations, we plot the results for $L_j = 0.1$, 0.333, and 0.567 at $A = 0.173$ and $\theta = -90$ deg in Fig. 8 and compare them with the baseline case. The streamlines of these three cases all clearly demonstrate a smaller separation bubble on the surface of the airfoil than the baseline case. In Fig. 8a, when suction is applied near the leading edge ($L_j = 0.1$), the separation is most effectively delayed, and hence, the separation bubble is much smaller than in the other cases. At $L_j = 0.567$, the only control effect of suction is to break the separation bubble into two smaller separation bubbles, but its lift increase is less than that for suction at location 0.1. Note from Fig. 8b that the pressure change near the leading-edge area is significant, and leading-edge suction changes the upper surface low-pressure zone more efficiently than downstream suction. Therefore, a location near the leading edge is the most effective place for a suction jet to manipulate the boundary layer to increase lift.

In Fig. 9, the effects caused by the changes of suction amplitude are investigated. The suction location is fixed at 0.1, and the suction angle is fixed at 90 deg. As suction amplitude increases from 0.01 to 0.2, the flow becomes more attached to the surface and a larger

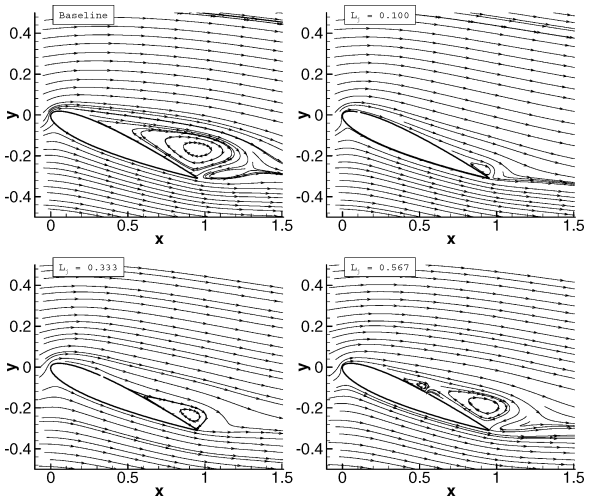

a)

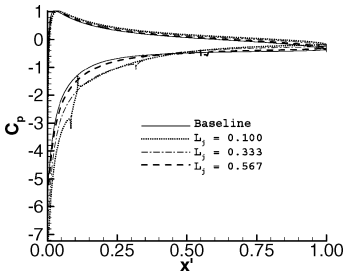

b)

Fig. 8 Control effects of suction at different locations, $L_j = 0.1$, 0.333, and 0.567, where $A = 0.173$ and $\theta = -90$ deg.

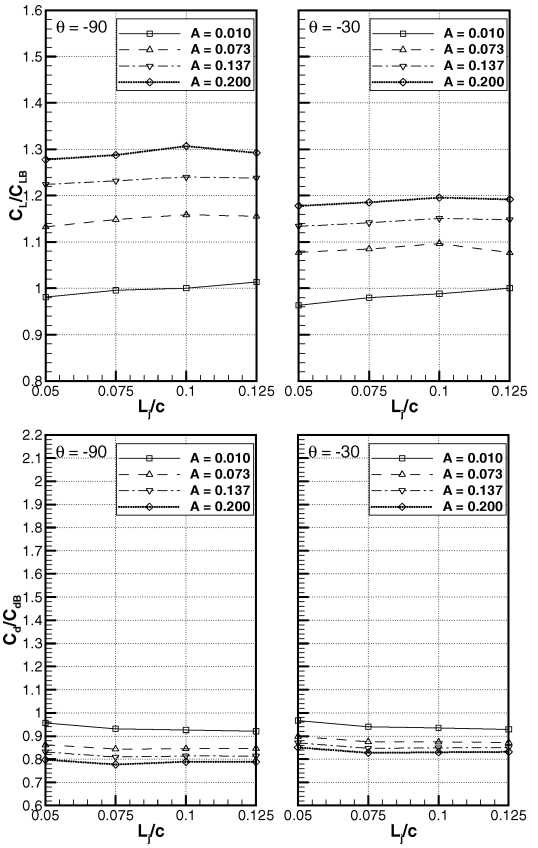

Fig. 10 Suction computation results on leading edge, $0.05 \le L_j \le 0.125$, $0.01 \le A \le 0.2$, and $\theta = -90$ and -30 deg.

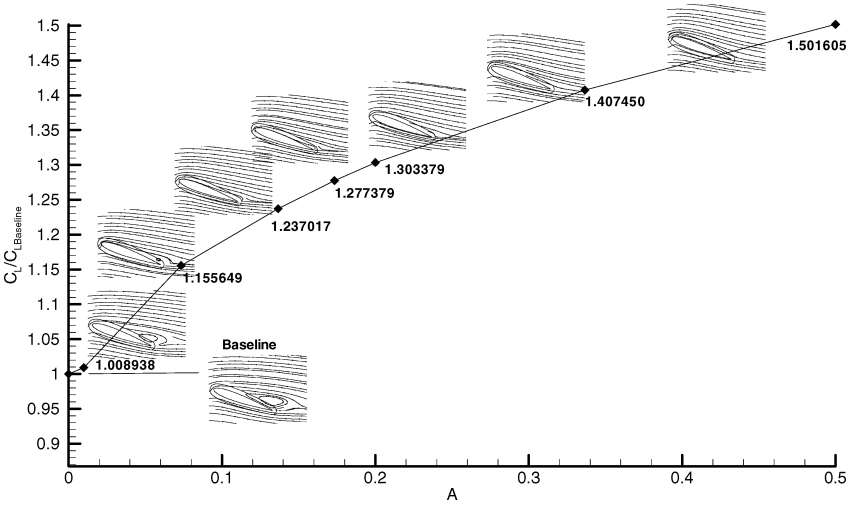

a)

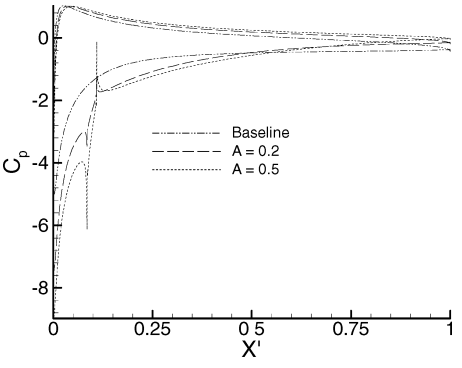

b)

Fig. 9 Control effects of suction at different amplitudes, $0 \le A \le 0.5$, $L_j = 0.1$, and $\theta = -90$ deg.

and lower pressure zone is created at the leading edge. The corresponding separation bubble also continues to decrease to where it is effectively eliminated at amplitude of 0.2. For amplitude greater than 0.2, the separation bubble remains suppressed; further increase in the lift coefficient is due to the continually decreasing pressure zone near the leading edge rather than changes in the downstream flow.

Figure 10 mainly focuses on the effects of suction near the leading edge. In this numerical study, the suction amplitude is limited to a smaller range: 0.01–0.2. As can be seen from Fig. 10, the increase of lift and drag does not seem to be affected by the location of the suction within this range, from $L_j = 0.05$ to 0.125. These results are consistent with several reported numerical and experimental works that demonstrated the effective control locations on the airfoil for suction jets. Examples include Dannenberg and Weiberg,[4] who studied the changing porous area suction that is located from the leading edge to the 0.03 chord length on airfoil upper surface; Weiberg and Dannenberg,[5] who studied the changing porous area suction that is located from the 0.02 chord length on the lower surface to the 0.07 chord length on the upper surface; Gilarranz and Rediniotis,[22] who studied a synthetic jet that is located at 0.115 chord length on the upper surface; and Hassan and Janakiram,[23] who studied a synthetic jet that is located at 0.13 chord length on the upper surface.

Blowing Control

From Fig. 11, the immediate observation regarding blowing effects is that downstream blowing at a smaller angle (30 deg) increases the lift and decreases the drag; however, leading-edge blowing has the opposite effect, not only decreasing the lift but also increasing the drag at the same time. Even though leading-edge blowing exerts negative effects on the lift and drag coefficients, these effects are much smaller than the favorable effects caused by

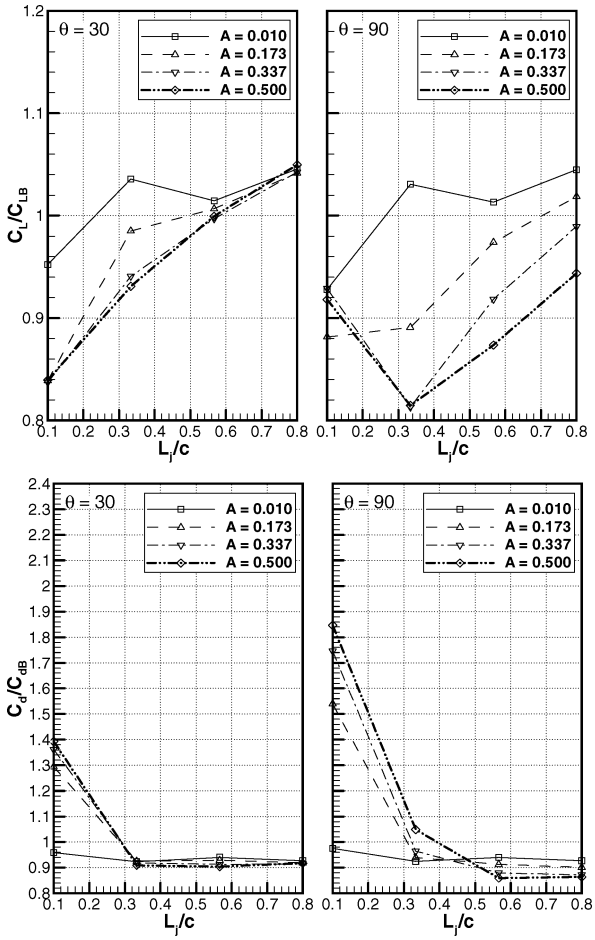

Fig. 11 Computation results of initial blowing study, $0.1 \le L_j \le 0.8$, $0.01 \le A \le 0.5$, and $\theta = 30$ and 90 deg.

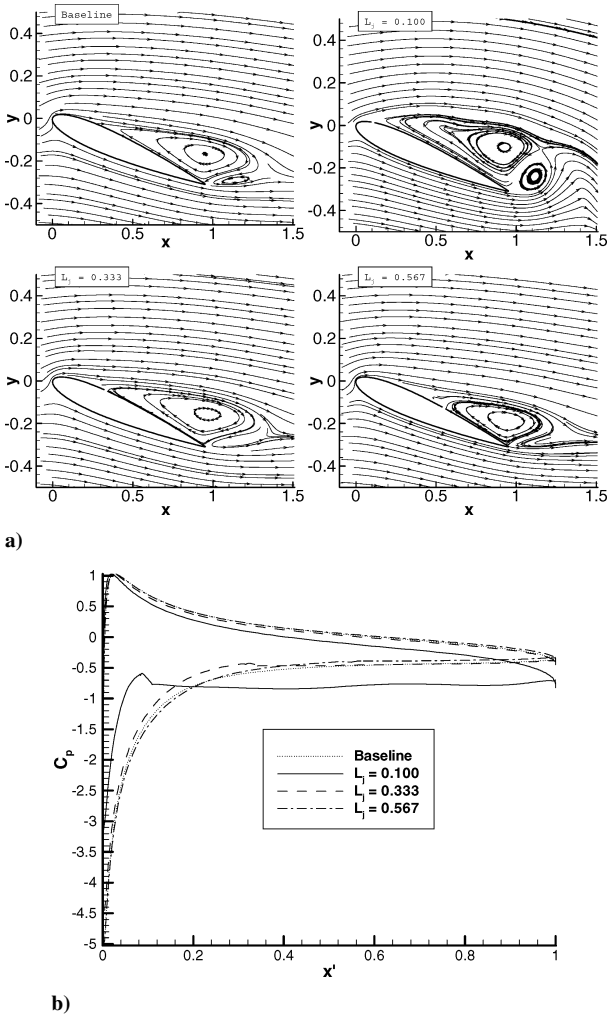

Fig. 12 Control effects of blowing at different locations, $L_j = 0.1, 0.333$, and 0.567, where $A = 0.173$ and $\theta = 90$ deg.

the jet suction. Therefore, we speculate that for the oscillatory blowing control on the leading edge, such as synthetic jet control, suction period is the dominant factor on increasing the lift and decreasing the drag. Another interesting phenomenon regarding drag is that when blowing amplitude increases near the leading edge, it increases; however, downstream drag decreases, even though the changes are slight. This observation will be confirmed in the following investigation after the blowing location range of interest is narrowed down to the leading edge and downstream region separately.

Blowing control on changing flow patterns at different locations are described in Fig. 12. The results for $L_j = 0.1$, 0.333, and 0.567 are plotted and compared with the baseline case. These cases are all under $A = 0.173$ and $\theta = 90$ deg conditions. Note from Fig. 12a that perpendicular blowing at location 0.1 creates a significantly different flow pattern compared with baseline cases: The separation bubble is significantly larger, and the circulation is larger, which makes the pressure after the jet location much lower. It can be correspondingly seen in Fig. 12b that the C_p curve with a blowing jet at location 0.1 is different from the baseline case, consistent with the changes of the separation bubble. The C_p value of the upper surface before the blowing jet significantly increases, and although the value after the jet decreases, the end result is a much smaller closed area within the C_p curve. This corresponds to a reduced lift compared to the baseline case. When blowing is moved downstream to locations 0.333 and 0.567, the separations are more suppressed than leading-edge blowing; only far downstream around 0.8 of chord length does blowing have a positive effect on lift as seen in Fig. 11.

Because we found little discussion of leading-edge blowing in previous research works, the focus is narrowed down to the effects of blowing near the leading edge in Fig. 13. It can be easily seen that

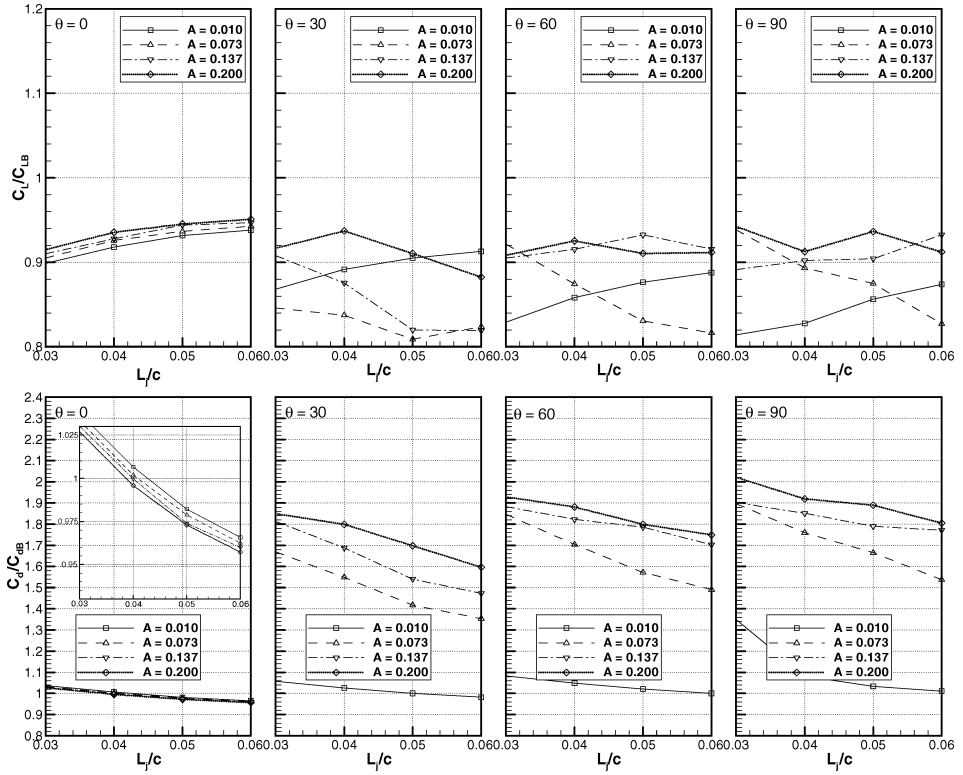

Fig. 13 Computation results for blowing on the leading edge, $0.03 \le L_j \le 0.06$, $0.01 \le A \le 0.2$, and $\theta = 0$, 30, 60, and 90 deg.

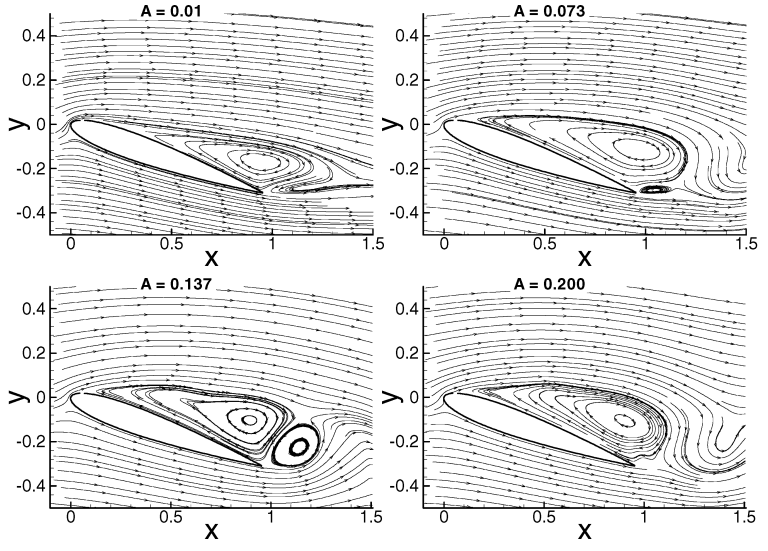

a)

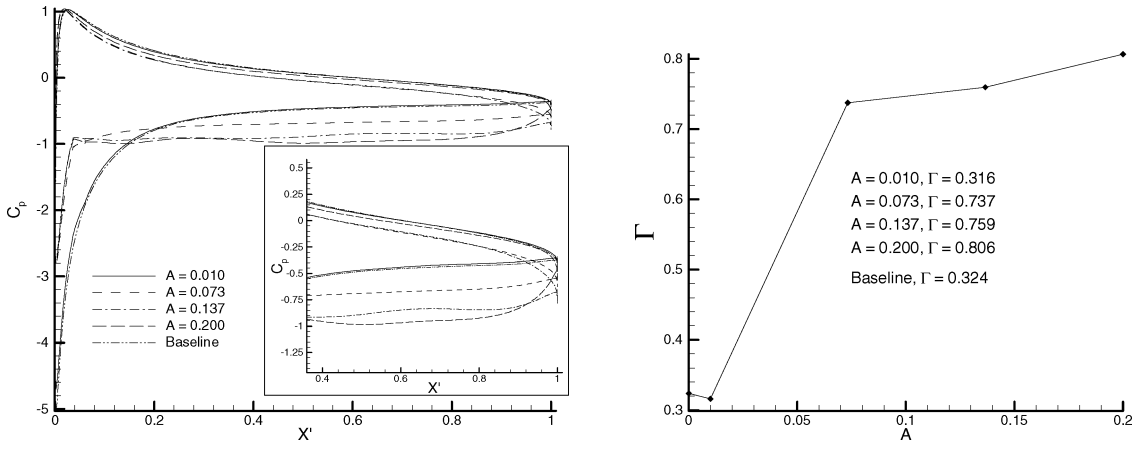

b) c)

Fig. 14 Control effects of blowing at different amplitudes, $0.01 \le A \le 0.5$, $L_j = 0.1$, and $\theta = 30$ deg.

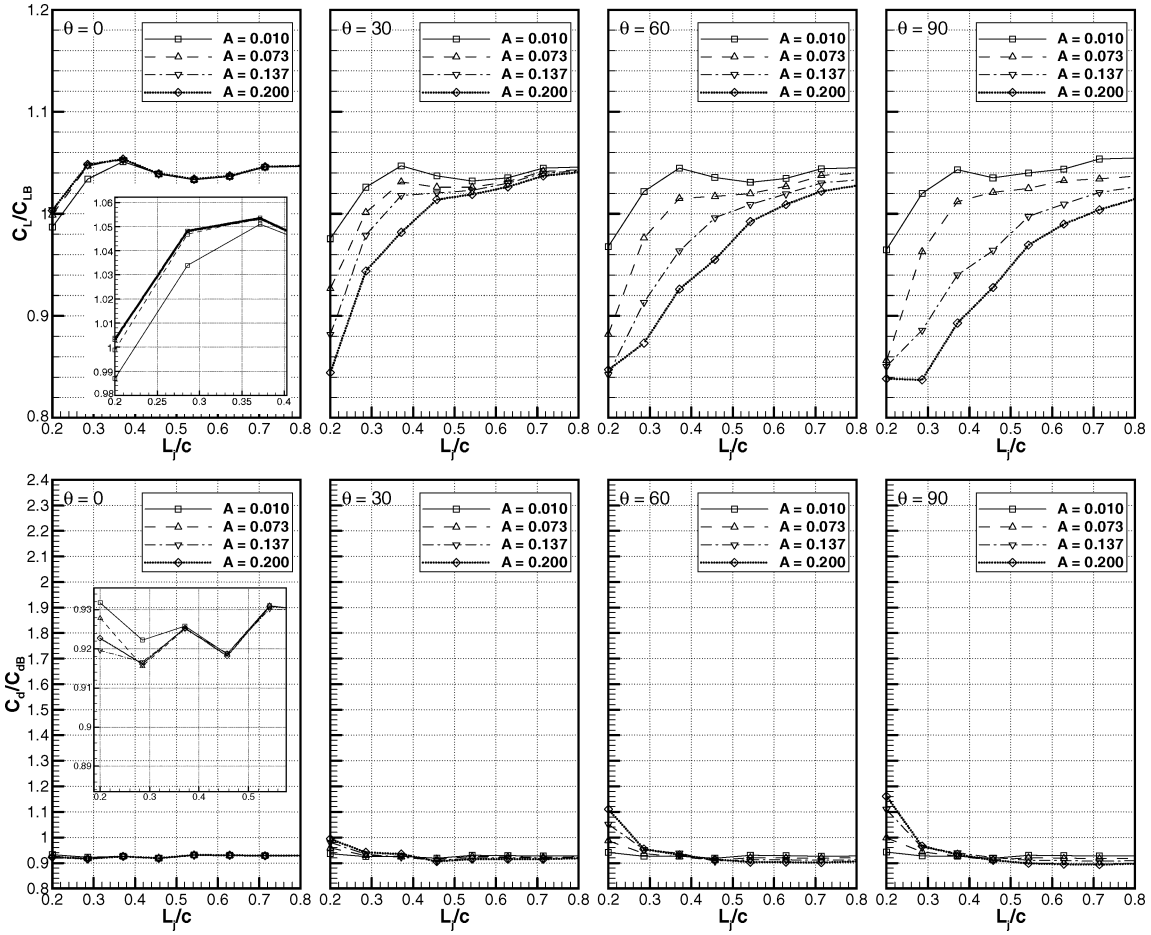

Fig. 15 Computation results for blowing on downstream, $0.2 \le L_j \le 0.8$, $0.01 \le A \le 0.2$, and $\theta = 0$, 30, 60, and 90 deg.

all of the end results of leading-edge blowing control are worse than baseline cases: All normalized lift values are smaller than 1.0, and most of the normalized drag values are larger than 1.0. There are three driving factors that together explain the lift and drag changes. The first factor is changes in the upper surface pressure, C_p, in the vicinity of the jet due to the direct effect of the blowing. The second factor is increased shear stress near the surface in the vicinity of the jet, increasing skin-friction drag and decreasing lift. The third factor is changes in the overall circulation about the airfoil, Γ, caused by the blowing modifying the flow around the separation bubble. The first factor increases the pressure on the airfoil upper surface near the leading edge, decreasing the lift and increases the drag in all of the cases. The second factor increases the drag and decreases the lift due to skin friction. The third factor decreases the airfoil upper surface pressure beneath the separation bubble downstream, increasing lift ($L = -\rho U \Gamma$) when the amplitude increases. Another interesting observation in Fig. 13 is that, when amplitude increases, the normalized drag of tangential (0 deg) blowing decreases slightly (insert of Fig. 13), but that of perpendicular (90-deg) blowing increases.

To explore the control effects of these driving factors in detail, Fig. 14 shows the changes in the flow due to amplitude at the location 0.05 of chord and the angle of 30 deg. It can be seen from Fig. 14 that the flow pattern at amplitude 0.01 is essentially the same as the baseline case except that the pressure near the leading-edge upper surface is slightly higher due to the blowing; the lift decrease at this point is primarily caused by skin-friction effects. When the amplitude goes from 0.01 to 0.073, C_p at the upper surface of leading edge increases dramatically (Fig. 14b). Meanwhile the circulation Γ around the separation bubble increases significantly (Fig. 14c), which in turn makes the circulation about the airfoil increasingly negative, which decreases the downstream upper surface C_p and thereby increases the lift. The net effects of these driving factors are that lift decreases and drag increases. For the amplitudes of 0.137 and 0.2, lift increases relative to the 0.073 case. The reason can be found in Figs. 14b and 14c. Near the leading edge, the upper surface pressure of these three amplitude cases are essentially the same, but the steady increase in circulation about the separation bubble flattens the downstream pressure curve; hence, the closed areas within C_p curve are larger, which means a larger lift. In no case, however, did the overall lift increase relative to the no-jet baseline due to leading-edge blowing.

In Fig. 15, the focus is shifted to the effects of blowing downstream, which ranges from 0.2 to 0.8. For downstream blowing, with fixed blowing location and blowing amplitude, tangential blowing is insensitive to amplitude changes and has a larger impact on increasing lift than other angles. These results indicate that there are two locations that are better for increasing the lift, one around 0.371 and the other around 0.8. The first location manipulates the separation bubble; the second location manipulates the trailing-edge vortex circulation. Another important observation in Fig. 15 is that the control effects generated by the smallest blowing amplitude of 0.01 are comparable in terms of drag reduction and generally better in terms of lift enhancement than those of larger amplitudes independent of the blowing angle. Therefore, whereas at high jet amplitude suction is clearly more effective, at smaller jet amplitudes downstream tangential blowing may be as or more advantageous.

Conclusions

In this work, we presented the numerical simulation results of suction and blowing control on a NACA 0012 airfoil at a Reynolds number of 5×10^5 and an angle of attack of 18 deg. When three parameters (jet location, amplitude, and angle) were changed over a wide range, specific ranges and values of interest were discovered and analyzed, and the following conclusions have been drawn.

First, from a mechanism perspective, suction is different from blowing. Suction takes the advantage of creating a larger and lower pressure, C_p, zone on the airfoil's upper surface to increase lift; hence, the flow is more attached and the profile drag decreases. Blowing is often counterproductive with most control results worse than the baseline case. Leading-edge blowing increases lift by generating greater circulation about the separation bubble and about the airfoil, but at the cost of significantly increasing leading-edge pressure; therefore, the flow is more detached and the profile drag increases. Downstream blowing can improve lift and drag characteristics, but smaller amplitudes are better than larger amplitudes.

Second, from an amplitude perspective, a larger amplitude unsurprisingly results in a larger impact on the flowfield around the airfoil, although for blowing that impact is a negative one in many cases. For perpendicular suction, the optimum control amplitudes range between 0.01 and 0.2; values exceeding 0.2 no longer manipulate the separation bubble for perpendicular suction. For downstream tangential blowing, smaller blowing amplitudes appear to be the most effective choice.

Third, when location and angle considerations are combined, perpendicular suction at leading edge (from 0.075 to 0.125) is better than other suction situations for increasing lift; in the case of blowing, tangential blowing at downstream locations (around 0.371 and 0.8) is better than other blowing situations for increasing lift.

References

[1]Williams, J., "A Brief History of British Research on Boundary Layer Control for High Lift," *Boundary Layer and Flow Control*, Pergamon, New York, 1961, pp. 74–103.

[2]Head, M. R., "History of Research on Boundary Layer Control for Low Drag in U.K.," *Boundary Layer and Flow Control*, Pergamon, New York, 1961, pp. 104–121.

[3]Flatt, J. "The History of Boundary Layer Control Research in the United States of America," *Boundary Layer and Flow Control*, Pergamon, New York, 1961, pp. 122–143.

[4]Dannenberg, R. E., and Weiberg, J. A., "Section Characteristics of a 10.5-Percent Thick Airfoil with Area Suction as Affected by Chordwise Distribution of Permeability," NASA TN 2847, Dec. 1952.

[5]Weiberg, J. A., and Dannenberg, R. E., "Section Characteristics of an NACA 0006 Airfoil with Area Suction Near the Leading Edge," NASA TN 3285, Sept. 1954.

[6]Wuest, W., "Theory of Boundary Layer Suction to Prevent Separation," *Boundary Layer and Flow Control*, Pergamon, New York, 1961, pp. 196–208.

[7]Smith, B. L., and Glezer, A., "The Formation and Evolution of Synthetic Jets," *Physics of Fluids*, Vol. 10, No. 9, 1998, pp. 2281–2297.

[8]Rizzetta, D. P., Visbal, M. R., and Stanek, M. J., "Numerical Investigation of Synthetic-Jet Flowfields," *AIAA Journal*, Vol 37, No. 8, 1999, pp. 919–927.

[9]Wu, J.-Z., Lu, X.-Y., Denny, A. G., Fan, M., and Wu, J.-M., "Post-Stall Flow Control on an Airfoil by Local Unsteady Forcing," *Journal of Fluid Mechanics*, Vol. 371, 1998, pp. 21–58.

[10]Nae, C., "Synthetic Jets Influence on NACA0012 Airfoil at High Angle of Attacks," AIAA Paper 98-4523, Aug. 1998.

[11]Hauser, T., Mattox, T. I., LeBeau, R. P., Dietz, H. G., and Huang, P. G., "High-Cost CFD on a Low-Cost PC Cluster," *Proceedings of ACM/IEEE SC2000*, Dallas, TX, Nov. 2000.

[12]Suzen, Y. B., and Huang, P. G., "Numerical Simulation of Wake Passing on Turbine Cascades," AIAA Paper 2003-1256, Jan. 2003.

[13]Suzen, Y. B., Huang, P. G., Volino, R. J., Corke, T. C., Thomas, F. O., Huang, J., Lake, J. P., and King, P. I., "A Comprehensive CFD Study of Transitional Flows in Low-Pressure Turbines Under a Wide Range of Operation Conditions," AIAA Paper 2003-3591, June 2003.

[14]Suzen, Y. B., and Huang, P. G., "Predictions of Separated and Transitional Boundary Layers Under Low-Pressure Turbine Airfoil Conditions Using an Intermittency Transport Equation," *Journal of Turbomachinery*, Vol. 125, No. 3, 2003, pp. 455–464.

[15]Menter, F. R., "Two-Equation Eddy-Viscosity Turbulence Models for Engineering Applications," *AIAA Journal*, Vol. 32, No. 8, 1994, pp. 1598–1605.

[16]Bardina, J. E., Huang, P. G., and Coakley, T. J., "Turbulence Modeling Validation, Testing and Development," NASA TM-110446, April 1997.

[17]Sheldahl, R. E., and Klimas, P. C., "Aerodynamic Characteristics of Seven Airfoil Sections Through 180 Degrees Angle of Attack for use in Aerodynamic Analysis of Vertical Axis Wind Turbines," Sandia National Labs., Rept. SAND80-2114, Albuquerque, NM, March 1981.

[18]Critzos, C. C., Heyson, H. H., and Boswinkle, R. W., Jr., "Aerodynamic Characteristics of NACA0012 Airfoil Section at Angles of Attack from 0° to 180°," NACA TN 3361, Jan. 1995.

[19]Jacobs, E., and Sherman, A., "Airfoil Section Characteristics as Affected by Variations of the Reynolds Number," NACA Rept. 586,231, 1937.

[20]Zaman, K. B. M. Q., McKinzie, D. J., and Rumsey, C. L., "A Natural Low-Frequency Oscillation of the Flow over an Airfoil Near Stalling Conditions," *Journal of Fluid Mechanics*, Vol. 202, 1989, pp. 403–442.

[21]McCroskey, W. J., "A Critical Assessment of Wind Tunnel Results for the NACA0012 Airfoil," NASA TM 100019, Oct. 1987.

[22]Gilarranz, J. L., and Rediniotis, O. K., "Compact, High-Power Synthetic Jet Actuators for Flow Separation Control," AIAA Paper 2001-0737, Jan. 2001.

[23]Hassan, A., and Janakiram, R. D., "Effects of Zero-Mass Synthetic Jets on the Aerodynamics of the NACA-0012 Airfoil," *Journal of the American Helicopter Society*, Vol. 43, No. 4, Oct. 1998.